




Highly thermally conductive graphene film produced using glucose under low-temperature thermal annealing

Jing Li^{1,2,*} , Xu-Yang Chen¹, Ru-Bai Lei¹, Jin-Feng Lai¹, Tong-Mei Ma¹, and Yang Li^{3,*}

¹ School of Chemistry and Chemical Engineering, South China University of Technology, Guangzhou 510641, China

² South China University of Technology-Zhuhai Institute of Modern Industrial Innovation, Zhuhai 519000, China

³ School of Mechanical and Automotive Engineering, South China University of Technology, Guangzhou 510641, China

Received: 8 December 2018

Accepted: 30 January 2019

Published online:

13 February 2019

© Springer Science+Business Media, LLC, part of Springer Nature 2019

ABSTRACT

Graphene films have attracted much attention as a heat dissipation material due to their unique thermal transfer behavior that exceeds that the performance of graphite. However, the very high thermal annealing temperature (~ 3000 °C) required to reduce the graphene oxide (GO) films leads to high manufacturing costs and restricts its broader application in thermal management applications. In this study, a modified-graphene (m-Gr) film was fabricated by vacuum-filtering GO suspensions with added glucose, followed by thermal annealing at 1000 °C. Oxygen-containing functional groups were effectively eliminated during annealing and activated carbon atoms from the decomposition of glucose molecules repaired defects in the graphene sheets to restore large areas of the π -conjugated structure. The as-obtained m-Gr films showed excellent in-plane thermal conductivity $\sim 1300 \text{ Wm}^{-1} \text{ K}^{-1}$ and much more efficient heat removal than pristine-reduced graphene oxide films. This high thermal conductivity of m-Gr films provides opportunities for their use in next-generation commercial electronics.

Introduction

The continuous miniaturization of components (and corresponding increase in power density) for electronics, aerospace instruments, and portable equipment has resulted in significant development of advanced materials that can conduct heat rapidly and

efficiently [1]. Traditional metal materials have satisfactory ductility, but poor thermal conductivity; for example, pure Cu (one of the metals with the highest heat conduction) has a thermal conductivity of only $400 \text{ Wm}^{-1} \text{ K}^{-1}$ at room temperature. Therefore, nonmetallic materials are being investigated as promising alternatives for achieving higher thermal conductivity. Although the thermal conductivity of

Address correspondence to E-mail: ljing@scut.edu.cn; meyangli@scut.edu.cn

high-quality diamond film can reach $2000 \text{ Wm}^{-1} \text{ K}^{-1}$, the harsh production conditions and high production cost limit large-scale application [2]. Graphite has a high basal heat conductivity of $\sim 2000 \text{ Wm}^{-1} \text{ K}^{-1}$ [3]; however, unprocessed graphite blocks cannot be directly used in the electronics industry due to their low thermal conductivity and tendency to shed powder causing a short circuit.

Graphene is a novel two-dimensional material consisting of single layers of sp^2 hybridized carbon atoms arranged in a honeycomb lattice. It was first successfully prepared from common graphite by micromechanical stripping in 2004 [4]. The thermal conductivity of suspended single-layer graphene at room temperature is in the range from 2000 to $5300 \text{ Wm}^{-1} \text{ K}^{-1}$, exceeding that of bulk graphite and diamond [5, 6]. Generally, since graphene oxide (GO) is a precursor of graphene and has good water solubility, the graphene materials can be easily prepared from aqueous GO solutions and subsequent thermal reduction [7, 8]. Hence, graphene has great potential as an alternative heat conduction material for effective thermal management [9]. For example, Shen et al. [10] fabricated ultrathin graphite-like graphene films with the high in-plane thermal conductivity of $1100 \text{ Wm}^{-1} \text{ K}^{-1}$ by graphitizing GO films at $2000 \text{ }^\circ\text{C}$. Xin et al. [11] showed that large-area freestanding graphene paper produced by high-temperature annealing ($2850 \text{ }^\circ\text{C}$) and mechanical pressing (300 MPa) possessed superior thermal conductivity ($\sim 1434 \text{ Wm}^{-1} \text{ K}^{-1}$). Peng et al. [12] reported that the debris-free giant graphene sheets subjected to the heat treatment at $3000 \text{ }^\circ\text{C}$ endowed the graphene film with a high thermal conductivity of $1940 \pm 113 \text{ Wm}^{-1} \text{ K}^{-1}$. Although graphene films with a thermal conductivity above $1000 \text{ Wm}^{-1} \text{ K}^{-1}$ were produced, such processes require an extremely high annealing temperature, leading to high energy consumption and high manufacturing costs.

In contrast with the above methods, a more attractive alternative would be to prepare highly thermally conductive graphene under milder condition, and some research efforts have been devoted to this issue. Renteria et al. [13] obtained the freestanding reduced graphene oxide film subjected to a high-temperature treatment of up to $1000 \text{ }^\circ\text{C}$ and the in-plane thermal conductivity of the film reached $61 \text{ Wm}^{-1} \text{ K}^{-1}$. Wu and Drzal [14] prepared graphene nanoplatelet paper using low-temperature thermal annealing ($340 \text{ }^\circ\text{C}$), followed by mechanical pressing

(10 MPa) to improve the thermal transport performance, resulting in paper with an in-plane thermal conductivity of $313 \text{ Wm}^{-1} \text{ K}^{-1}$. Analogously, Hou et al. [15] directly fabricated pure graphene-graphene composites from few-layer graphene nanosheets (GNs), and improvement in the performance was achieved by thermal annealing at $1060 \text{ }^\circ\text{C}$. However, the observed thermal conductivity of the annealed GN-GN film was in the range of $220\text{--}390 \text{ Wm}^{-1} \text{ K}^{-1}$. It is clear that these graphene films still have relatively low thermal conductivity. Song et al. [16] showed that when the annealing temperature increased from $1000 \text{ }^\circ\text{C}$ to $1200 \text{ }^\circ\text{C}$, the thermal conductivity of thermally reduced graphene oxide films improved from ~ 860 to $\sim 1040 \text{ Wm}^{-1} \text{ K}^{-1}$, respectively. Although the thermal conductivity of graphene films has been significantly improved, high temperatures ($\sim 1200 \text{ }^\circ\text{C}$) are still required during processing. Therefore, it is still a significant challenge to prepare graphene films with thermal conductivity much higher than $1000 \text{ Wm}^{-1} \text{ K}^{-1}$ when the annealing temperatures are not more than $1000 \text{ }^\circ\text{C}$.

Here, we solve the problem by adding glucose to the GO film to repair defects of graphene sheets during thermal annealing at $1000 \text{ }^\circ\text{C}$. Thermal conductivity of the modified-graphene (m-Gr) film was 62.5% greater than that of the pristine-reduced graphene oxide (rGO) film, ascribing to its highly ordered crystalline and conjugated structure. In addition, the heat treatment temperature was only $1000 \text{ }^\circ\text{C}$, far lower than the current graphitization temperature ($\sim 3000 \text{ }^\circ\text{C}$), which is expected to significantly reduce production costs. Consequently, our contribution provides a simple and convenient approach for preparing graphene films with remarkable heat transfer performance under low processing temperature.

Materials and methods

Materials preparation

Natural graphite powder (325 mesh) was purchased from Tengshengda Tansu Jixie Co. Ltd., Qingdao, China. Glucose was purchased from Sinopharm Chemical Reagent Co. Ltd., Shanghai, China. All other chemicals used in this study were purchased from the Guangzhou Chemical Reagents Factory, Guangzhou, China.

Preparation of GO and GO-glucose (GO-glu)

GO was prepared using the improved Hummers method [17]. An aqueous GO suspension ($\sim 4.5 \text{ mg ml}^{-1}$) was treated in an ultrasonic cleaner (Shanghai Kedao SK7200H) at 53 kHz and 350 W for 60 min, followed by centrifugation (3000 rpm for 20 min) to remove impurities. The thickness of GO sheet was measured to be around 1.0 nm by AFM, as shown in Fig. S1a (supporting information). This value includes the thicknesses of monolayer graphene and the functional groups on its basal plane, indicating the GO was a single-layer structure [18]. In addition, their lateral dimensions were in the range of several hundreds of nanometers to several micrometers according to their SEM image as shown in Fig. S1b (supporting information). GO-glu mixture was prepared by dissolving 25 mg glucose powder in 6.5 ml of the prepared GO suspension under vigorous agitation (600 rpm) for 10 min.

Fabrication of GO-glu and m-Gr film

The GO-glu mixture (6.5 ml) was vacuum-filtered with a vacuum system equipped with a mixed cellulose filter membrane (50 mm diameter, 0.45 μm pore size). The obtained film was dried at 50 $^{\circ}\text{C}$ for 2 h before being peeled off the membrane, and we eventually obtained the GO-glu film.

In order to prepare the m-Gr film, the GO-glu film was reduced by thermal annealing at 1000 $^{\circ}\text{C}$ at a heating rate of 5 $^{\circ}\text{C min}^{-1}$; the target temperature was maintained for 2 h under argon (purity, 99.999%) flow of 100 ml min^{-1} . Thereafter, the sample was naturally cooled to ambient temperature under the argon flow. As a comparison, the GO and rGO films were prepared using the same method described above without glucose added.

Characterization

The morphology of the film samples was characterized using scanning electron microscopy (SEM) with a Hitachi UHR FE-SEM SU8200 system operated at 10.0 kV. The high-resolution transmission electron microscopy (HR-TEM, JEOL-JEM 2100F) was used to demonstrate the defects restoration. X-ray diffraction (XRD, D8 Advance, AXS) with Cu $K\alpha$ radiation ($\lambda = 0.15406 \text{ nm}$) was performed over the range of

5 $^{\circ}$ –50 $^{\circ}$. X-ray photoelectron spectroscopy (XPS) measurements were performed using a Physical Electronics Axis Ultra DLD spectrometer with a monochromatic Al $K\alpha$ radiation at a power of 75 W and a voltage of 15 kV. Laser confocal Raman microscopy was performed using a Horiba Jobin-Yvon LabRAM ARAMIS system with He-Ne laser excitation at 532 nm. Fourier transform infrared spectroscopy (FTIR) was performed using a Bruker Tensor 27 system; the samples were pressed with KBr powder to form pellets for testing test.

The in-plane thermal diffusivity (D) of all samples was determined using a laser flash apparatus (Netzsch LFA 447) operated at room temperature in a vacuum of 0.01 Pa. In this method, the test sample was cut into round shape with diameter of 25.4 mm, which is the ideal size for the sample holder plate. First, the sample was heated by light pulse (voltage 270 V; pulse width medium, 0.18 ms), and then the resulting temperature rise at four different positions is measured using an infrared detector. For adiabatic conditions, the thermal diffusivity is determined by analyzing the temperature versus time curve based on the following equation: $D = 0.1388 \times d^2 \times t_{50}^{-1}$, where D is the thermal diffusivity, mm^2/s ; d is the thickness of the tested sample, mm; t_{50} is time at 50% of the temperature increase, measured at the rear of the tested sample, s. The measuring principle (Netzsch LFA 447) is shown in Fig. S9 (supporting information), and the schematic of in-plane sample holder is shown in Fig. S10 (supporting information).

The density (ρ) of sample was measured by dividing the mass (m) by the volume (V). The m was available by weighing the round sample with a diameter of 25.4 mm using electronic precision balance (Sartorius, Quintix125D-1CN) with a graduation value of 0.01 mg. The volume was determined by the products of round flake area and thickness of the sample. The thickness of the sample was determined by a pachometer (Shanghai Siwei Instrument Manufacturing co., Ltd.). To ensure the accuracy of measurement of thickness, the five thickness values at different points on the measured sample were obtained, and their average value was adopted as the thickness of the sample.

The specific heat capacity (C_p) was obtained using differential scanning calorimetry (DSC; Netzsch DSC 204 F1). The measurement was conducted using sapphire method according to the equation:

$(DSC_{sam} - DSC_{bsl}) / (DSC_{std} - DSC_{bsl}) = (C_{psam} \times M_{sam}) / (C_{pstd} \times M_{std})$, where DSC_{sam} , DSC_{bsl} , and DSC_{std} are the ordinate of the DSC curves corresponding to the sample, blank specimen, and standard specimen, respectively. C_{psam} and C_{pstd} are the specific heat of the sample and standard specimens, respectively. M_{sam} and M_{std} are the mass of the sample and standard specimens, respectively.

Finally, the thermal conductivity (k) of the sample was calculated using $k = D \times \rho \times C_p$. The three pieces of films of each sample were tested to give the value of k .

The tensile strength tests were performed using an Instron 5565 tensile tester with a strain rate of 0.1 mm min^{-1} . The bending test was carried out on a homemade endurance testing equipment with a repeated bending/releasing angle of 180° , as shown in Fig. S2 (supporting information).

Results and discussion

As shown in the schematic diagrams in Fig. 1a, in a typical procedure, the glucose was dissolved in the GO suspension with the assistance of vigorous agitation to produce the parent GO-glu mixture. Since the glucose contains sufficient hydroxyl groups that interact with oxygen groups via hydrogen bonding on the surface and edge of GO nanosheets, it can effectively inhibit re-stacking of GO, which helps form a homogeneous dispersion. The prepared GO-glu dispersion can be stable for 180 days without precipitation, as shown in Fig. S3 (supporting information). Loss of glucose molecules through the membrane during vacuum filtering of the GO-glu mixture was limited by the deposition of large GO sheets, which could not pass through the pores. A hybrid GO-glu film was obtained by deposition of uniform and compact GO sheets on the filter membrane surface during vacuum filtration, with the glucose molecules adsorbed and intercalated between GO sheets. As shown in Fig. 1b, c, the surface of the GO-glu film was extremely smooth and the film showed excellent flexibility. Then, the m-Gr film was produced by thermal annealing at 1000°C in an Ar atmosphere. As shown in Fig. 1d, e, a representative as-obtained m-Gr film (40-mm diameter) exhibited a metallic luster with typical flexibility. Further, the m-Gr film could be bent without apparent degradation and touched without powder

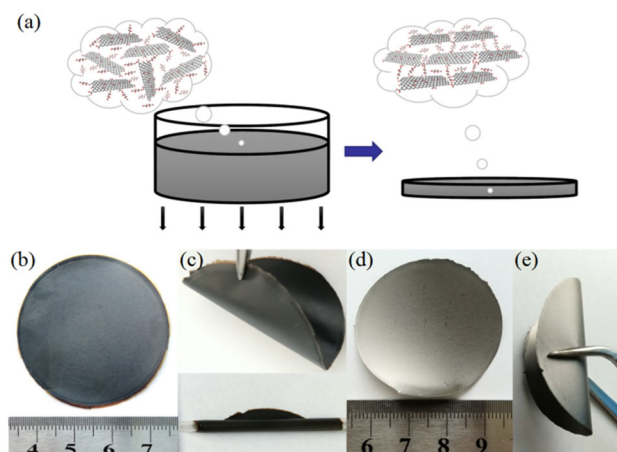
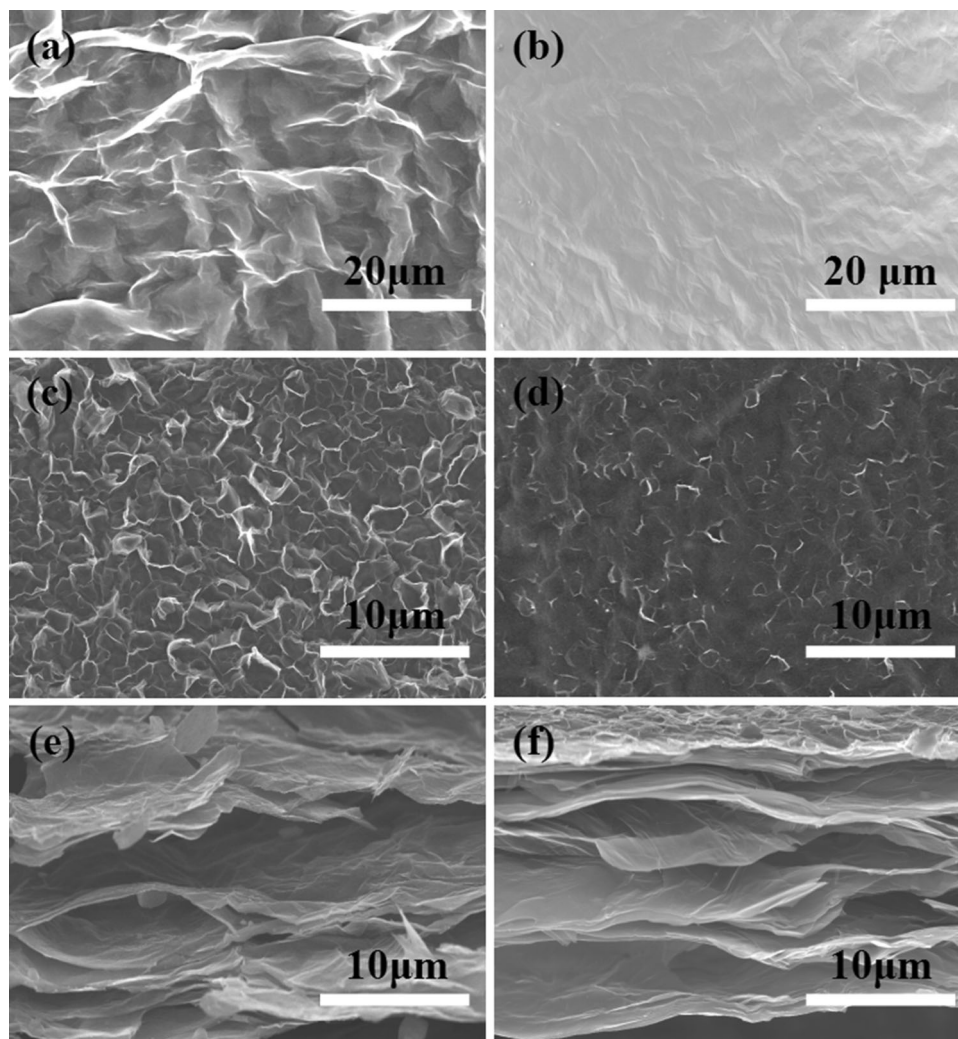


Figure 1 a Schematic diagram of the vacuum filtration fabrication of hybrid GO-glu films from solution. Photographs of a b, c hybrid GO-glu films and d, e m-Gr films after thermal annealing at 1000°C .

shedding, which satisfied the basic requirements for heat dissipation applications.

The SEM was employed to observe the morphology of the as-prepared films. As shown in Fig. 2a, the surface of the pristine GO film was very rough, generally containing a large number of wrinkles and turbulent stacking. However, as shown in Fig. 2b, the surface of GO-glu film was flatter and smoother except for some slight wrinkles, which was attributed to the fact that the GO sheets adsorbed with glucose could be arranged in a more orderly manner during film formation. After thermal annealing at 1000°C , as shown in Fig. 2c, d, there were many cracks on the surface of the rGO film, indicating that moderate thermal treatment was not effective in repairing cracks. However, the m-Gr film showed a more integral surface with few cracks which showed that most of the defects were repaired. The thermal annealing at 1000°C was much lower than the graphitization temperature ($\sim 3000^\circ\text{C}$) and, hence, did not significantly increase the crystallinity of graphene and repair the defects of graphene structure. However, the intercalated glucose formed graphene using the GO nanosheets as templates during the thermal treatment [19], and also served as an additional carbon source to stitch and repair the graphene sheets [20, 21]. Meantime, the cross-section morphology of rGO and m-Gr are shown in Fig. 2e, f, respectively. Although both samples have a well-packed layered structure, more voids and cracks were observed on the rGO than the m-Gr, indicating

Figure 2 SEM images of surface morphology of **a** GO and **b** GO-glu films. The surface morphology (**c**, **d**) and the cross section (**e**, **f**) of rGO and m-Gr films after thermal annealing, respectively.



that the m-Gr film had a more homogenous graphene layer and a denser structure (as shown in Table. S1, supporting information).

The structural evolution of GO-glu to m-Gr was further analyzed by XRD. As shown in Fig. 3, the diffraction pattern of GO-glu had a peak at $2\theta = 10.2^\circ$, indicating a larger interlayer spacing (d-spacing) of 0.866 nm than that of GO (0.804 nm at $2\theta = 11.0^\circ$). This was attributed to numerous glucose molecules being attached to the GO sheet surfaces via hydrogen bonding and many oxygen-containing functional groups being introduced onto the carbon basal plane [22]. This phenomenon proves that glucose can play an effective role in preventing aggregation and random stacking of GO nanosheets. After the thermal annealing, the sharp peaks located at 10.2° for GO-glu and 11.0° for GO disappeared, while a new intense feature with diffraction peaks at

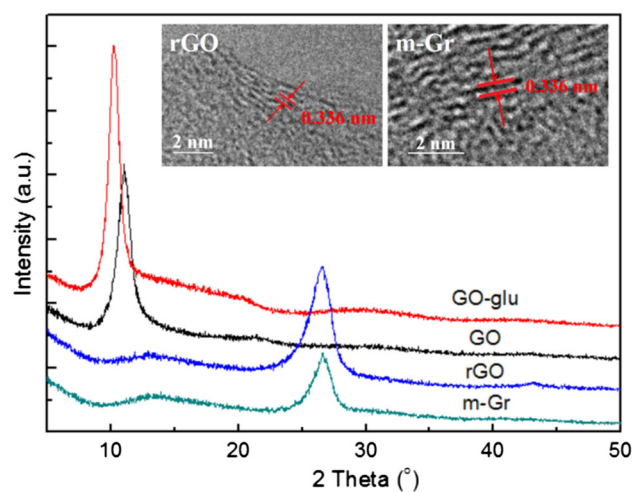


Figure 3 XRD patterns of GO, GO-glu, rGO, and m-Gr films. The inset shows interlayer spacing of rGO and m-Gr films measured by TEM.

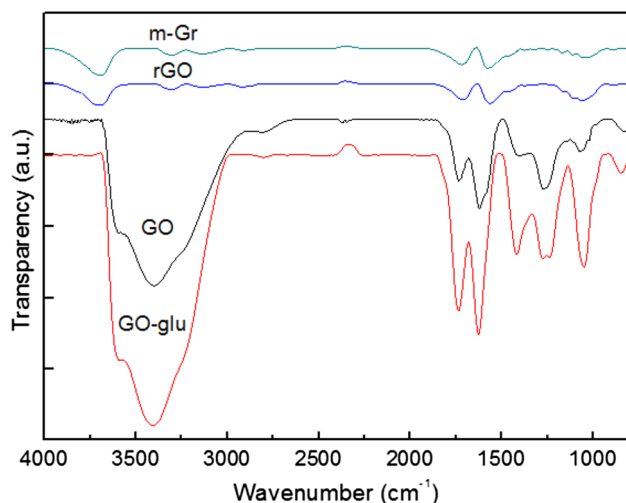


Figure 4 FTIR spectrum of GO, GO-glu, rGO, and m-Gr films.

$\sim 26.5^\circ$ was observed with a d-spacing of 0.336 nm in the rGO and m-Gr films corresponding with the TEM results (as shown in the inset in Fig. 3); this indicated that the decomposition products of glucose did not increase the d-spacing between the graphene layers, which agreed well with the SEM results. Moreover, the d-spacing of 0.336 nm is similar to that of the typical (002) diffraction peak of pristine natural graphite [23]. This phenomenon is attributed to complete decomposition of oxygen-containing functional groups and glucose molecules on the surfaces of GO sheets. The removal of oxygen is a very important step during annealing as sp^2 clusters in GO-glu are separated by oxygen atoms, which will result in significant phonon scattering during thermal conduction. Accordingly, the elimination of oxygenated groups can restore more sp^2 clusters and reconstitute a larger area of the π -conjugated structure [24].

The FTIR spectroscopy was used to evaluate the surface functional groups of the GO, GO-glu, rGO, and m-Gr films, as shown in Fig. 4. The GO and GO-glu samples had various types of oxygen-containing groups, such as O–H (3406 cm^{-1}), C=O (1735 cm^{-1}), OH^- (1410 cm^{-1}), C–OH (1275 cm^{-1}), C–O (1050 cm^{-1}), and physically adsorbed water (1626 cm^{-1}) [25, 26]. Comparing the FTIR spectrum of GO-glu with that of m-Gr, the peaks of many oxygen-containing functional groups nearly disappeared after thermal treatment at $1000\text{ }^\circ\text{C}$ [27], coinciding with the thermogravimetric curve in Fig. S4 (supporting information). However, a small number of residual oxygen atoms remained in the m-Gr film,

such as ethers, carbonyl, and quinone, which can only be fully removed at higher temperature [28, 29]. Correspondingly, the carbon–oxygen atomic ratio (C/O) increased from 3 in GO-glu, to 33 in m-Gr, as detected by elemental analysis, coinciding with from XPS result, as shown in Fig. S5 (supporting information). Meanwhile, it is worth noting that the C=C stretching vibration (at 1575 cm^{-1} , normally observed in benzene) was clearly observed in the m-Gr sample, implying recovery of the conjugated C=C system [16]. In addition, the FTIR spectrum of m-Gr was almost identical to that of rGO, demonstrating that the glucose completely decomposed into carbon during thermal treatment, as shown in Fig. S6 (supporting information).

The texture of the m-Gr film was investigated using Raman spectroscopy. As shown in Fig. 5a, the most intense features were the D band at $\sim 1354\text{ cm}^{-1}$ and the G band at $\sim 1595\text{ cm}^{-1}$. The D band is related to structural disorders and defects on the carbon basal plane, while the G band is typical of sp^2 -hybridized carbon networks [30]. Further, the D/G intensity ratios (I_D/I_G) of GO and GO-glu were about 1.02 and 1.03, respectively, indicating that the addition of glucose had no effect on the structure of the GO sheets. After thermal annealing, the I_D/I_G of rGO increased to about 1.33, which was related to the removal of functional groups and formation of defects [31]. However, the I_D/I_G of m-Gr was only 1.04 which was much smaller than that of rGO. This definitively demonstrated that the defects on the graphene nanosheets were largely repaired during the heat treatment due to the addition of glucose [32]. According to Cançado's equation [33], the calculated in-plane crystallite size (L_a) of rGO and m-Gr reaches 14.5 nm and 18.4 nm, respectively. That is, the crystallite size of m-Gr was 17.4% higher than that of rGO, which can effectively reduce phonon scattering and enhance thermal conductivity. Consistent with Raman spectra, HR-TEM analysis (Fig. S7, supporting information) further confirmed a less defective and better-ordered structure of m-Gr compared with rGO.

Further, the chemical bonding was characterized by XPS, as shown in Fig. 5b, c. The C 1s spectra of rGO and m-rGO films can be deconvoluted into five peaks arising from $sp^2\text{C}$ ($\sim 284.5\text{ eV}$), $sp^3\text{C}$ ($\sim 285.1\text{ eV}$), C–O ($\sim 286.3\text{ eV}$), C=O ($\sim 287.5\text{ eV}$), and –COO ($\sim 288.8\text{ eV}$) [22]. In contrast to rGO, the peak associated with sp^3 -hybridized

C clearly reduced and that of sp^2 -hybridized C increased in m-Gr, confirming that a large number of defects were effectively repaired during thermal annealing due to the presence of glucose. In addition to these analyses, other comparative experiments were undertaken to demonstrate that the defects in the graphene sheets could be effectively repaired during heat treatment with the addition of glucose, as shown in Fig. S8 (supporting information). Obviously, the I_D/I_G of the samples decreased from 1.48 to 1.10 due to the addition of glucose.

The results of the laser flash analysis conducted to determine the in-plane thermal conductivity of copper foil, rGO films, and m-Gr films, as shown in Fig. 6, and the corresponding detailed datum were shown in Table S2, S3 and S4 (supporting information). The in-plane thermal conductivity of pristine

rGO film was only $\sim 800 \text{ Wm}^{-1} \text{ K}^{-1}$ (at 30°C). However, a clear increase of $\sim 62.5\%$ in the in-plane thermal conductivity was observed for the m-Gr film. The m-Gr film possessed excellent thermal conductivity, up to $1300 \text{ Wm}^{-1} \text{ K}^{-1}$, nearly 3.2 times higher than that of copper foil ($\sim 401 \text{ Wm}^{-1} \text{ K}^{-1}$). Although, this value is much lower than that of individual graphene sheets, possibly resulting from the residual oxygen atoms, vacancy defects and thermal contact resistance between graphene sheets. However, it is worth noting that the low annealing temperature of 1000°C demonstrated in our method is highly advantageous as a practical energy-efficient processing solution, which could greatly reduce production costs of highly thermally conductive graphene film.

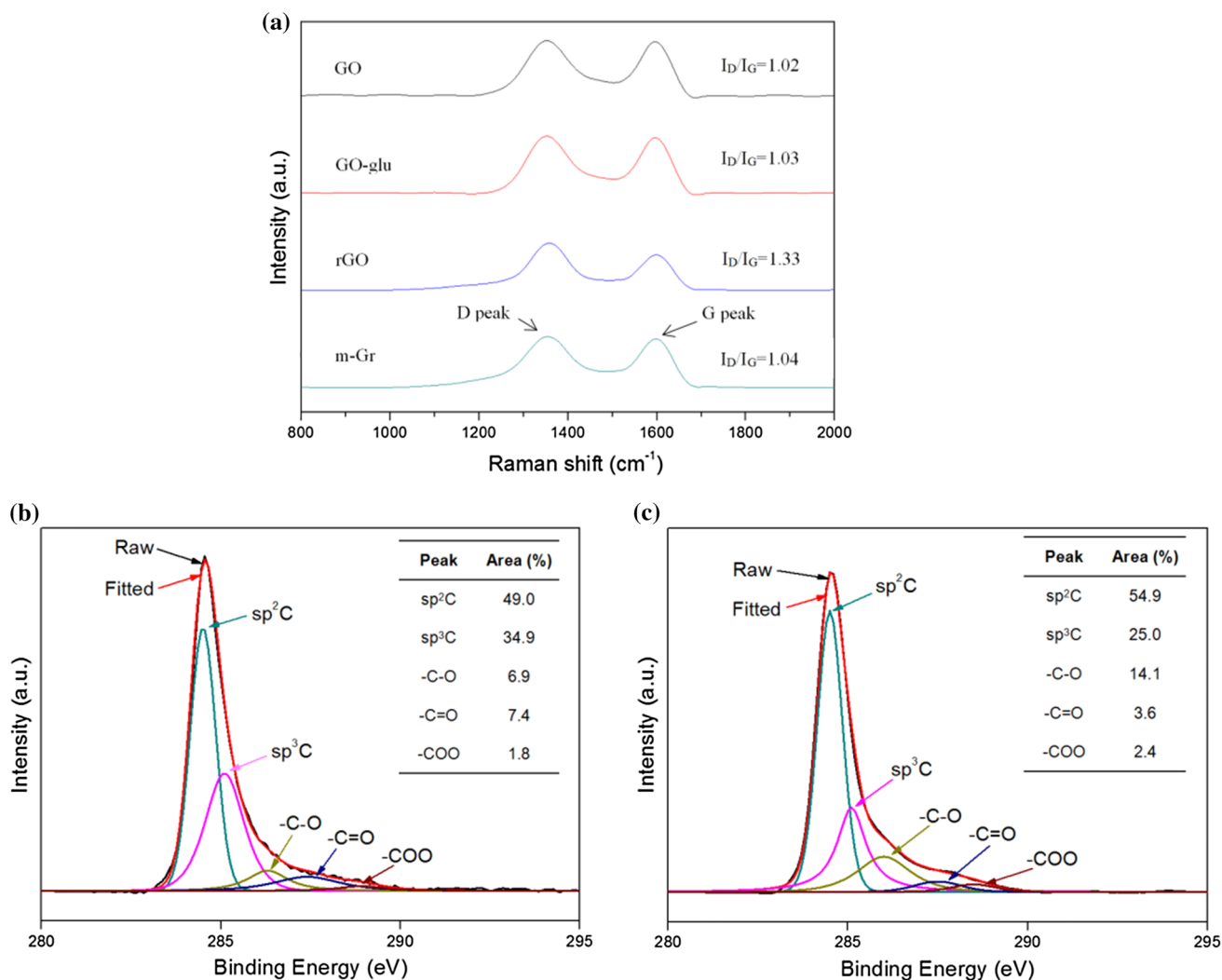


Figure 5 a Raman spectra of GO, GO-glu, rGO, and m-Gr films. Deconvoluted XPS C1 s spectra of the b rGO and c m-Gr films.

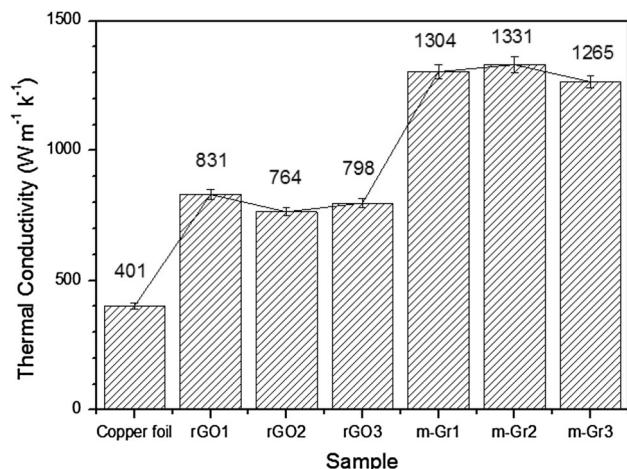


Figure 6 In-plane thermal conductivity of copper foil, rGO films (rGO1, rGO2, and rGO3), and m-Gr films (m-Gr1, m-Gr2, and m-Gr3).

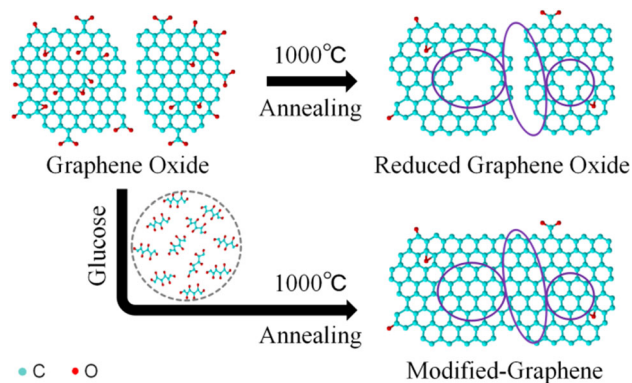


Figure 7 Schematic diagram of the defect repair mechanism during the fabrication of the m-Gr film.

We propose that the crucial factor determining the high thermal conductivity of the m-Gr film was the abundance of high-quality graphene sheets resulting from their defects being repaired during thermal annealing via the process shown in the schematic diagram in Fig. 7. The process of removing oxygen species provided active sites for external carbon doping of the graphene sheets, which can effectively reduce the vacancy concentration in sp^2 -hybridized carbon lattice domains. Heat conduction in carbon materials is dominated by phonons, so larger area of sp^2 -hybridized clusters can effectively decrease phonon scattering during heat transfer [34]. In addition, the single layers of graphene synthesized from glucose during heat treatment may play an important role in stitching adjacent graphene nanosheets together, which is very important for eliminating thermal contact resistance between the sheets [21, 35, 36]. The product of decomposed glucose increased the grain size of the graphene sheets and provided a better channel for phonon transport, thus leading to a higher in-plane thermal conductivity.

The mechanical properties of the m-Gr film were investigated using bending and tensile tests in order to evaluate the suitability of the m-Gr films for potential applications. As shown in Fig. 8a, the tensile strength was ~ 21 MPa, close to the value for commercial flexible graphite paper (~ 20 MPa). The good tensile strength of the m-Gr film was attributed to the orderly stacks and fewer defects in the graphene sheets after removal of abundant oxygen groups. In addition, as shown in Fig. 8b, the m-Gr films showed a constant electrical resistance over

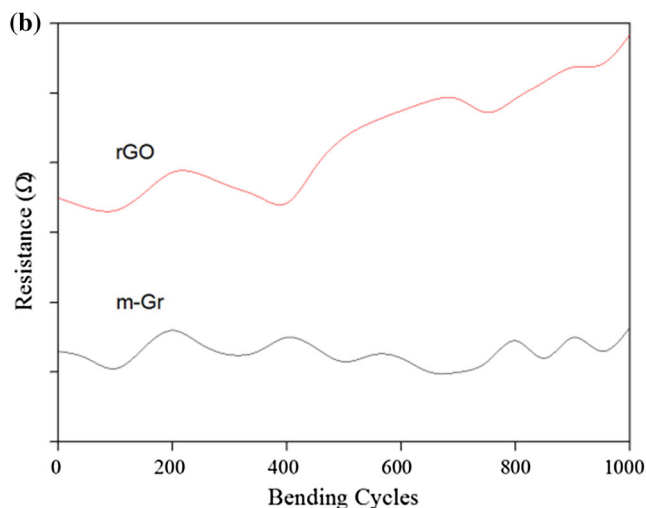
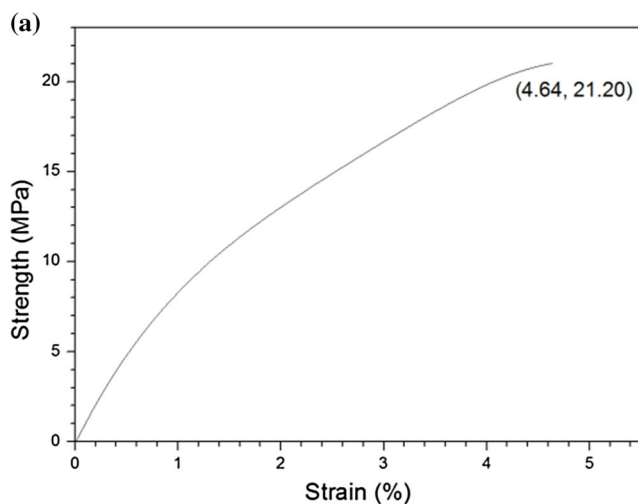


Figure 8 **a** Tensile curve of the m-Gr film. **b** Electrical resistances of rGO and m-Gr films over 1000 bending cycles ($R5/180^\circ$).

more than 1000 cycles of 180° bending, indicating that the inner structure was not broken. In comparison, the rGO film showed an obvious increase in resistance after 500 bending cycles, implying that the inner structure had been destroyed. Despite the thermal conductivity and mechanical properties of the m-Gr film being inferior to those of graphene films reported in recent literature [12, 37, 38], the remarkable enhancement in thermal conductivity and flexibility of our m-Gr films demonstrates that the addition of glucose and the use of low-temperature thermal annealing is a promising path for fabricating graphene-based films for thermal dissipation applications.

Conclusion

A new strategy for preparing high-thermal-conductivity m-Gr films was presented using low-temperature thermal annealing of GO-glu films. The lower thermal annealing temperature (~ 1000 °C) compared to other graphitization temperature provides the opportunity for energy-efficient and environmentally friendly industrial production. In addition, the m-Gr films had both high thermal conductivity (~ 1300 Wm⁻¹ K⁻¹) and good tensile strength (~ 21 MPa). The glucose performed a repair function during the reduction process; the carbon produced by the decomposition of glucose repaired vacancies in the graphene sheet matrix and also stitched together adjacent nanosheets to restore large areas of the π -conjugated structure, which could increase the overall thermal conductivity of the macroscopic graphene films. In conclusion, we have demonstrated an effective and valuable material preparation method (using mild production conditions) for the application of highly thermally conductive graphene films for thermal management applications.

Acknowledgements

The authors acknowledge financial support by the “13th Five-Year Plan” Civil Aerospace Technology Pre-Research Project of the State Administration of Science, Technology, and Industry for National Defense (501-01-2018-0167, A2180150); the Fundamental Research Funds for the Central Universities (D2175010); and the Joint Fund for Equipment Pre-

Research of Ministry of Education of China (6141A02022520).

Compliance with ethical standards

Conflict of interest The authors declare that they have no conflict of interest.

Electronic supplementary material: The online version of this article (<https://doi.org/10.1007/s10853-019-03406-x>) contains supplementary material, which is available to authorized users.

References

- [1] Balandin AA (2011) Thermal properties of graphene and nanostructured carbon materials. *Nat Mater* 10(8):569–581
- [2] Sukhadolau AV, Ivakin EV, Ralchenko VG, Khomich AV, Vlasov AV, Popovich AF (2005) Thermal conductivity of CVD diamond at elevated temperatures. *Diam Relat Mater* 14:589–593
- [3] Malekpour H, Chang KH, Chen JC, Lu CY, Nika DL, Novoselov KS et al (2014) Thermal conductivity of graphene laminate. *Nano Lett* 14(9):5155–5161
- [4] Novoselov KS, Geim AK, Morozov SV, Jiang D, Zhang Y, Dubonos SV et al (2004) Electric field effect in atomically thin carbon films. *Science* 306:666–669
- [5] Balandin AA, Ghosh S, Bao W, Calizo I, Teweldebrhan D, Miao F et al (2008) Superior thermal conductivity of single-layer graphene. *Nano Lett* 8(3):902–907
- [6] Nika DL, Balandin AA (2017) Phonons and thermal transport in graphene and graphene-based materials. *Rep Prog Phys* 80(3):036502
- [7] Dikin DA, Stankovich S, Zimney EJ, Piner RD, Dommett GHB, Evmenenko G et al (2007) Preparation and characterization of graphene oxide paper. *Nature* 448:457–460
- [8] Gao X, Jang J, Nagase S (2010) Hydrazine and thermal reduction of graphene oxide: reaction mechanisms, product structures, and reaction design. *J Phys Chem C* 114(2):832–842
- [9] Kargar F, Barani Z, Balinskiy M, Magana AS, Lewis JS, Balandin AA (2019) Dual-functional graphene composites for electromagnetic shielding and thermal management. *Adv. Electron. Mater.* 5(1):1800558
- [10] Shen B, Zhai W, Zheng W (2014) Ultrathin flexible graphene film: an excellent thermal conducting material with efficient EMI shielding. *Adv Funct Mater* 24(28):4542–4548
- [11] Xin G, Sun H, Hu T, Fard HR, Sun X, Koratkar N et al (2014) Large-area freestanding graphene paper for superior thermal management. *Adv Mater* 26(26):4521–4526

- [12] Peng L, Xu Z, Liu Z, Guo Y, Li P, Gao C (2017) Ultrahigh thermal conductive yet superflexible graphene films. *Adv Mater* 29(27):1700589
- [13] Renteria JD, Ramirez S, Malekpour H, Alonso B, Centeno A, Zurutuza A et al (2015) Strongly anisotropic thermal conductivity of free-standing reduced graphene oxide films annealed at high temperature. *Adv Funct Mater* 25(29):4664–4672
- [14] Wu H, Drzal LT (2012) Graphene nanoplatelet paper as a light-weight composite with excellent electrical and thermal conductivity and good gas barrier properties. *Carbon* 50(3):1135–1145
- [15] Hou Z-L, Song W-L, Wang P, Meziani MJ, Kong CY, Anderson A et al (2014) Flexible graphene–graphene composites of superior thermal and electrical transport properties. *ACS Appl Mater Interfaces* 6(17):15026–15032
- [16] Song N-J, Chen C-M, Lu C, Liu Z, Kong Q-Q, Cai R (2014) Thermally reduced graphene oxide films as flexible lateral heat spreaders. *J Mater Chem A* 2(39):16563–16568
- [17] Kang D, Shin HS (2012) Control of size and physical properties of graphene oxide by changing the oxidation temperature. *Carbon Lett* 13(1):39–43
- [18] Chen J, Li YR, Huang L, Li C, Shi GQ (2015) High-yield preparation of graphene oxide from small graphite flakes via an improved Hummers method with a simple purification process. *Carbon* 81(1):826–834
- [19] Li X-H, Kurasch S, Kaiser U, Antonietti M (2012) Synthesis of monolayer-patched graphene from glucose. *Angew Chem* 51(38):9689–9692
- [20] Cheng M, Yang R, Zhang L-C, Shi Z-W, Yang W, Wang D-M et al (2012) Restoration of graphene from graphene oxide by defect repair. *Carbon* 50(7):2581–2587
- [21] Li H-L, Dai S-C, Miao J, Wu X, Chandrasekharan N, Qiu H-X et al (2018) Enhanced thermal conductivity of graphene/epolyimide hybrid film via a novel “molecular welding” strategy. *Carbon* 126:319–327
- [22] Chang Y-Z, Han G-Y, Xiao Y-M, Zhou H-H, Dong J-H (2017) A comparative study of graphene oxide reduction in vapor and liquid phases. *New Carbon Mater* 32(1):21–26
- [23] Vallés C, Núñez JD, Benito AM, Maser WK (2012) Flexible conductive graphene paper obtained by direct and gentle annealing of graphene oxide paper. *Carbon* 50(3):835–844
- [24] Mattevi C, Eda G, Agnoli S, Miller S, Mkhoyan KA, Celik O et al (2009) Evolution of electrical, chemical, and structural properties of transparent and conducting chemically derived graphene thin films. *Adv Funct Mater* 19(16):2577–2583
- [25] Wang J, Ran R, Sunarso J, Yin C, Zou H, Feng Y et al (2017) Nanocellulose-assisted low-temperature synthesis and supercapacitor performance of reduced graphene oxide aerogels. *J Power Sour* 347:259–269
- [26] Zhu C, Guo S, Fang Y, Dong S (2010) Reducing sugar: new functional molecules for the green synthesis of graphene nanosheets. *ACS Nano* 4(4):2429–2437
- [27] Fang Y, Luo B, Jia Y, Li X, Wang B, Song Q et al (2012) Renewing functionalized graphene as electrodes for high-performance supercapacitors. *Adv Mater* 24(47):6348–6355
- [28] Figueiredo JL, Pereira MFR, Freitas MMA, Órfão JJM (1999) Modification of the surface chemistry of activated carbons. *Carbon* 37(9):1379–1389
- [29] Chen C-M, Huang J-Q, Zhang Q, Gong W-Z, Yang Q-H, Wang M-Z et al (2012) Annealing a graphene oxide film to produce a free standing high conductive graphene film. *Carbon* 50(2):659–667
- [30] Ferrari AC, Meyer JC, Scardaci V, Casiraghi C, Lazzeri M, Mauri F et al (2006) Raman spectrum of graphene and graphene layers. *Phys Rev Lett* 97(18):187401
- [31] Bagri A, Mattevi C, Acik M, Chabal YJ, Chhowalla M, Shenoy VB (2010) Structural evolution during the reduction of chemically derived graphene oxide. *Nat Chem* 2(7):581–587
- [32] Eigler S, Dotzer C, Hirsch A (2012) Visualization of defect densities in reduced graphene oxide. *Carbon* 50(10):3666–3673
- [33] Cançado LG, Takai K, Enoki T, Endo M, Kim YA, Mizusaki H (2006) General equation for the determination of the crystallite size L_a of nanographite by Raman spectroscopy. *Appl Phys Lett* 88(16):163106
- [34] Sheng Z-H, Shao L, Chen J-J, Bao W-J, Wang F-B, Xia X-H (2011) Catalyst-free synthesis of nitrogen-doped graphene via thermal annealing graphite oxide with melamine and its excellent electrocatalysis. *ACS Nano* 5(6):4350–4358
- [35] Zhang J, Shi G, Jiang C, Ju S, Jiang D (2015) 3D bridged carbon nanoring/graphene hybrid paper as a high-performance lateral heat spreader. *Small* 11(46):6197–6204
- [36] Zhuo H, Hu Y-J, Tong X, Chen Z-H, Zhong L-X, Lai H-H et al (2018) A supercompressible, elastic, and bendable carbon aerogel with ultrasensitive detection limits for compression strain, pressure, and bending angle. *Adv Mater* 30(18):1706705
- [37] Ding J, ur Rahman O, Zhao H, Peng W, Dou H, Chen H et al (2017) Hydroxylated graphene-based flexible carbon film with ultrahigh electrical and thermal conductivity. *Nanotech*. 28:(39)LT01-9
- [38] Wang N, Samani M-K, Li H, Dong L, Zhang Z-W, Su P et al (2018) Tailoring the thermal and mechanical properties of graphene film by structural engineering. *Small* 14(29):1801346

Publisher’s Note Springer Nature remains neutral with regard to jurisdictional claims in published maps and institutional affiliations.